Appl. Phys. B 70, 139–149 (2000) / Digital Object Identifier (DOI) 10.1007/s003409900099

Applied Physics B
Lasers
and Optics

Cavitation bubble behavior and bubble–shock wave interaction near a gelatin surface as a study of in vivo bubble dynamics

T. Kodama[1,*], **Y. Tomita**[2]

[1] Wellman Laboratories of Photomedicine, Massachusetts General Hospital, Harvard Medical School, 55 Fruit Street - WEL 224, Boston, MA 02114-2696, USA
(Fax: +1-617/726-3192, E-mail: kodama@helix.mgh.harvard.edu)
[2] Faculty of Education, Hokkaido University of Education, Hakodate, 1-2 Hachiman-cho, Hakodate, Hokkaido 040-8567, Japan
(Fax: +81-138/44-4307, E-mail: tomita@cc.hokkyodai.ac.jp)

Received: 8 December 1998/Revised version: 21 May 1999/Published online: 19 August 1999

Abstract. The collapse of a single cavitation bubble near a gelatin surface, and the interaction of an air bubble attached to a gelatin surface with a shock wave, were investigated. These events permitted the study of the behavior of in vivo cavitation bubbles and the subsequent tissue damage mechanism during intraocular surgery, intracorporeal and extracorporeal shock wave lithotripsy. Results were obtained with high-speed framing photography. The cavitation bubbles near the gelatin surface did not produce significant liquid jets directed at the surface, and tended to migrate away from it. The period of the motion of a cavitation bubble near the gelatin surface was longer than that of twice the Rayleigh's collapse time for a wide range of relative distance, $L/R_{\max}$, excepting for very small $L/R_{\max}$ values (L was the standoff distance between the gelatin surface and the laser focus position, and $R_{\max}$ was the maximum bubble radius). The interaction of an air bubble with a shock wave yielded a liquid jet inside the bubble, penetrating into the gelatin surface. The liquid jet had the potential to damage the gelatin. The results predicted that cavitation-bubble-induced tissue damage was closely related to the oscillatory bubble motion, the subsequent mechanical tissue displacement, and the liquid jet penetration generated by the interaction of the remaining gas bubbles with subsequent shock waves. The characteristic bubble motion and liquid jet formation depended on the tissue's mechanical properties, resulting in different damage mechanisms from those observed on hard materials.

PACS: 87.00; 43.25.Y

Pulsed ultraviolet and infrared lasers have been used in angioplasty, dermatology, ophthalmology, dentistry, urology, and orthopedic surgery. The laser beams are conventionally delivered to tissue by optical fibers or articulated optics. Laser energy can be strongly absorbed in tissue, producing shock waves and cavitation bubbles. The intensity of the shock waves and the cavitation bubbles depends on the characteristics of the laser beams employed [1]. The interior of the cavitation bubble is considered to be filled with vaporized tissue and gases dissolved in tissue. The collapse of the cavitation bubble becomes more intense as increasing in the surrounding liquid pressure and their rebounds are usually accompanied by shock wave radiation [2, 3]. The cavitation bubbles become gas bubbles through rectified diffusion of dissolved gases into the bubbles. The gas bubbles can remain for an extremely long time, thereby the interaction of the remaining gas bubbles with subsequent optical breakdown-induced shock waves is generated, producing liquid jet impacts. The impulsive pressures caused by these jet impacts are assumed to be directly or indirectly related to tissue damage during many optical and thermal processes involved in the biological tissue response [4]. Cavitation bubbles and the remaining gas bubbles which are associated with tissue damage have also been reported in extracorporeal shock wave lithotripsy (ESWL) [5–8].

In the case of laser lithotripsy, the maximum size of the cavitation bubbles was 4–8 mm in diameter for the pulsed-dye laser [9, 10], and 6 mm for the Q-switched Nd:YAG laser [10]. For an electrohydraulic apparatus (ESWL), the maximum bubble size was up to 14 mm in diameter [10]. Changes in tissue echogenicity were used to measure the in vivo cavitation thresholds during ESWL [11, 12], which were observed in a human liver parenchyma, remained from 40 s to 6 min after shock wave doses [12].

Cavitation bubbles change their behavior, depending on the dynamic properties of surrounding materials [13–15]. Cavitation bubbles near a rigid surface migrate toward the surface, producing liquid jets to the surface, while cavitation bubbles near a free surface migrate away from the surface, producing liquid jets in the opposite direction against the surface. The liquid jet formation depends on the motion of the liquid around the cavitation bubble that is excluded by the generation of the cavitation bubble. When a cavitation bubble exists near a boundary, the excluded liquid finally converges on a point, conserving the momentum given by the cavitation bubble generation during the bubble collapse. This convergence increases the stagnation pressure of the point, and

* Corresponding author

results in the large deformation of the bubble surface near the point, leading to the liquid jet formation [16].

The interaction of a shock wave with a gas bubble generates a liquid jet within the bubble [3, 7, 8, 17–19]. Under certain conditions, two liquid jets are formed within a gas bubble [18]. The liquid jet formation depends on the interacting shock wave profile, the initial bubble shape, the initial bubble size, and the bubble arrangement. The direction of the liquid jet does not always coincide with the shock wave direction [3, 17, 19].

Human tissue can be regarded as one of viscoelastic boundaries, which is dynamically nonlinear, anisotropic, and inhomogeneous. Thus, the behaviors of in vivo cavitation bubbles are assumed to be different from those observed near rigid and free surfaces. Furthermore, characteristic bubble-collapse-induced impulsive pressures depend on the dynamic properties of the surrounding tissue.

The aim of this paper is to investigate systematically the behavior of the bubbles near a gelatin surface, as a model of in vivo bubble dynamics during intracorporeal and extracorporeal shock wave lithotripsy, and intraocular surgery. The principle investigative tool employed was high-speed photography.

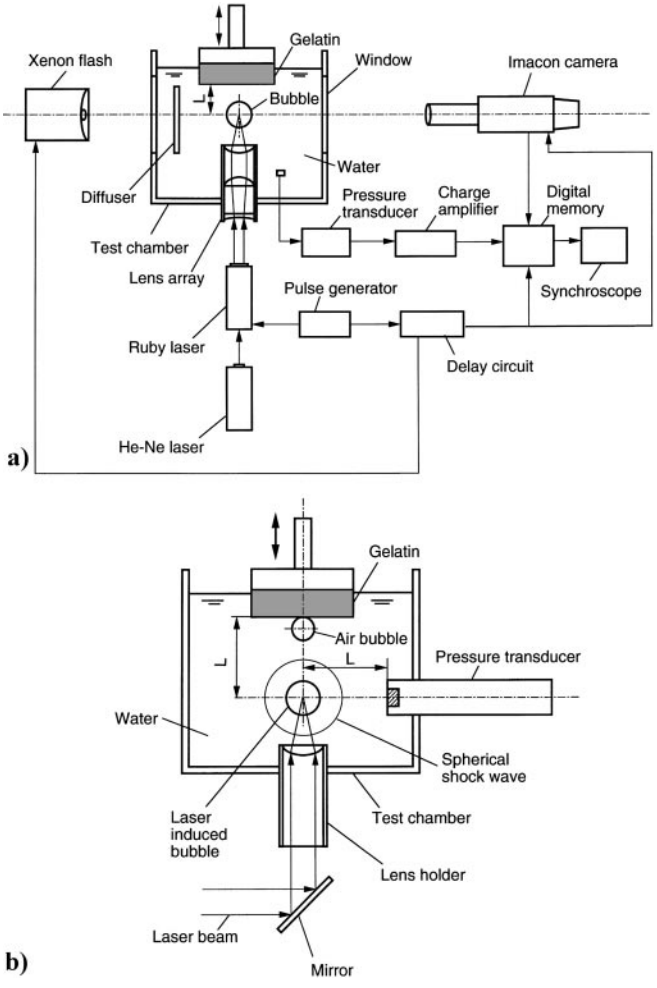

Fig. 1a,b. Schematic descriptions of the experimental setup. **a** Collapse of a cavitation bubble near a gelatin surface. **b** Interaction of an optical breakdown-induced shock wave with a single air bubble attached to a gelatin surface

1 Methods

Schematic descriptions of the experimental set up are shown in Fig. 1a,b. Figure 1a is an observation of the collapse of a bubble near a gelatin surface. This simulates the behavior of a cavitation bubble during intraocular surgery, intracorporeal and extracorporeal shock wave lithotripsy. Figure 1b shows the interaction of a shock wave with an air bubble attached to a gelatin surface. This gives information about intracorporeal and extracorporeal lithotripsy, intraocular surgery, and thrombolysis with revascularization of cerebral embolisms by the liquid jet impact [20]. Experiments were conducted in a stainless steel chamber (240 mm × 240 mm × 300 mm). The chamber was filled with tap water at room temperature, $T_0 = 291$ K, under atmospheric pressure, $P_0 = 101.3$ kPa. The saturated vapor pressure of the water, P_v, was 2064.4 Pa. The density of the water, ϱ_0, was 998.6 Kgm^{-3}. The tap water was supplied into the chamber through a filter with elements of 5 μm. The water surface tension was measured to be $7.2 \times 10^{-2}\,\mathrm{N\,m}^{-1}$ [21]. A ruby laser (Japan Science Engineering Co. Ltd., Japan, NGP 60 MP, 60 MW, wavelength 694 nm, pulse width 30 ns) and twin pulsed ruby lasers (Japan Science Engineering Co. Ltd., Japan, NAL-707TS 1, wavelength 694 nm, pulse width 30 ns) were employed [22].

1.1 Gelatin

Solid gelatin (Wako Pure Chemical Industries Ltd. Japan, LEN-0459) was used to mimic tissue. The gelatin was transparent, being suitable for observing phenomena that occurred within it. The solid gelatin was dissolved 10%, 20%, and 30% by weight in water at 333 K and then cast in a mold (35 mm × 150 mm × 70 mm). The mold surfaces were covered with a thin polyvinylidene chloride film of 5 μm. After slow cooling to reduce shrinkage, the gelatin layer was cut into pieces (25 mm × 25 mm × 8 mm). The acoustic impedance of the gelatin at 294 K was $1.62 \times 10^6\,\mathrm{kg\,m}^{-2}\,\mathrm{s}^{-1}$ for 10%, $1.80 \times 10^6\,\mathrm{kg\,m}^{-2}\,\mathrm{s}^{-1}$ for 20%, and $2.02 \times 10^6\,\mathrm{kg\,m}^{-2}\,\mathrm{s}^{-1}$ for 30% [23]. The impedance of the 10% gelatin was similar to that of human arteries, blood, liver, kidney, and other organs [24]. The impedance of the 20% gelatin was close to that of muscle and the 30% gelatin was for gallstone [25]. According to the one-dimensional acoustic theory [26], the normal incident intensity transmission coefficient at the water–gelatin interface was 99.8% for 10%, 99.0% for 20%, and 97.6% for 30%. For that reason the effect of wave reflection from the gelatin surface on the bubble collapse could be neglected. The gelatin was immersed in water from above. The immersion time of the gelatin was restricted to be less than 4 min to keep the degree of swelling of the gelatin. The swelling rate of the 10%–30% gelatin was less than 1.05 for four min. There was no difference in the behavior of the bubble when the thickness of the gelatin was over 6 mm, thus the bubble collapse was assumed to be independent of the gelatin thickness, unless its width was extremely small. Therefore, an 8-mm thickness of gelatin plate was employed.

The gelatin was supposed to be one-dimensional viscoelastic damping system as follows [27],

$$m\ddot{\eta} + \lambda\dot{\eta} + k\eta = F(t)\ , \qquad (1)$$

where m was the mass, λ was the viscous damping coefficient, k was the spring constant, $F(t)$ was the transitional impulsive force. These parameters were non-dimensionalized as follows,

$$m^* = m/(\rho_0 R_{\max}^3)$$
$$\lambda^* = \lambda/(R_{\max}^2\sqrt{\rho_0(P_0 - P_v)})$$
$$k^* = k((P_0 - P_v)R_{\max}) \,, \qquad (2)$$

where P_0 was the pressure in liquid at infinity, P_v was the saturated vapor pressure of the liquid at infinity, ρ_0 was the liquid density at the infinity, and $R_{\max}$ was the maximum bubble radius. When a modal analysis was applied for the gelatin employed in the paper, the non-dimensionalized parameters (m^*, λ^*, k^*) were (20.0, 3.0, 1.0) for 10%, (21.3, 11.1, 4.9) for 20%, and (22.8, 25.2, 18.4) for 30% [28]. The Young's modulus, Y, of the gelatin was determined by the linear relationship between the stress and the strain. The gelatin had a thickness of 6.1–7.0 mm. After the gelatin was immersed in water at 294 K for four min, it was placed on a digital balance (American Scientific Products, USA, 2-6000, readability is 0.1 g) at room temperature of 295 K. An aluminum rod with a diameter of 2.94 mm that was attached on a micrometer (Newport Co., USA, 423) was placed on the gelatin, then, the rod was lowered into the gelatin. The force was read from the digital balance after every 100 μm. The measured Young's modulus was $Y = 0.043 \pm 0.002$ MPa ($n = 3$) for 10%, $Y = 0.163 \pm 0.003$ MPa ($n = 3$) for 20%, and $Y = 0.304 \pm 0.012$ MPa ($n = 3$) for 30%. The Young's modulus of a human's renalparenchyma is 0.057 MPa, a human's stomach is 0.52 MPa [29], and a thoracic aorta is 0.0047–0.043 MPa [30]. These values have the same values as those of the gelatin employed.

1.2 Laser-induced cavitation bubbles near gelatin surfaces

The center of the gelatin surface was placed over the laser focal point (Fig. 1a). The laser beam was introduced through the lens holder inserted from the bottom of the test chamber and focused at a stand-off distance, L, from the gelatin surface. About 4 mJ of energy from a pulsed ruby laser was needed to produce a cavitation bubble with a 1-mm radius [22]. In the present experiment, the minimum relative distance was $L/R_{\max} = 0.062$. Pressure signals generated in synchronization with the motion of a cavitation bubble in water were used to confirm the generation and size of the cavitation bubble. A pressure transducer (Kistler Instrumente AG, Switzerland, Model 603B, with a 5.55-mm-diameter sensitive element, a resonant frequency of 400 kHz, and a rise time of 1 μs) was used for monitoring the overpressure, P_s, of the shock wave. The signals were amplified with a charge amplifier (Kistler Instrumente AG, Switzerland, Type 5007), stored in a digital memory (Iwatsu Electric Co. Ltd., DM-703), and displayed on a synchroscope (Iwatsu Electric Co. Ltd., Japan, SS-5415A, 1 MΩ (32 pF)). It was noted that the actual overpressure values recorded by the transducer were lower because the rise time of 1 μs of the transducer was longer compared with the rising times and the durations of shock wave pressures to be measured.

1.3 Interaction of air bubbles with laser-induced shock waves

A single air bubble with a given size was carefully placed under the center of the gelatin surface using a syringe (see Fig. 1b). Optical observations recorded that cavitation bubbles having mean radius of 0.15–0.38 mm were induced near the focus in water of an extracorporeal lithotripter with a 20 MPa pressure [31]. Intracorporeal shock wave lithotripter induces a cavitation bubble with the radius of 4.2 mm [9]. In the present paper, it was supposed that a gas bubble radius, R_e, of 0.36–0.74 mm would remain during intracorporeal and extracorporeal shock wave lithotripsy treatment. In the ophthalmic surgery, the remaining gas bubbles are hardly ever larger than 0.08 mm in radius [4]. However, the obtained results may explain some aspects of such a small bubble collapse with a shock wave during ophthalmic surgery. The center of the bubble was on the normal axis through the laser focal point. The stand-off distance, L, between the gelatin surface and the focal point was kept at 7.5 mm. The laser-induced breakdown in water produces a spherical shock wave and a cavitation bubble. The shock wave impacted on the air bubble attached to the gelatin surface. A pressure transducer (Kistler Instrumente AG, Switzerland, Model 603B, with a 5.55-mm-diameter sensitive element, a resonant frequency of 400 kHz, and a rise time of 1 μs), positioned at the same distance, L, was used for monitoring the overpressure. The measured overpressures were 2.8–4.2 MPa. The shock waves used in ESWL consist of positive pressures of 8–114 MPa and negative pressures of 2–9.9 MPa [5]. The pressure values used in the paper correspond to the values in the far zone from the focus point in ESWL. The energy E_c of the cavitation bubble is given by

$$E_c = \frac{4}{3}\pi(P_0 - P_v)R_{\max}^3 \,. \qquad (3)$$

The laser-induced cavitation bubbles had the maximum radii of $R_{\max} = 2.60$–4.17 mm. Thus, E_c was varied from 2.2 mJ to 9.7 mJ.

1.4 High-speed photography

The behavior of the collapsing bubbles was recorded with a high-speed camera (John Hadland Ltd., UK, Imacon 790) in framing mode; the frame rate was varied from 100 000 frames s^{-1} to 500 000 frames s^{-1}. A xenon flash lamp with a 200-μs pulse duration was used as a light source. The photography was controlled with a delay circuit. An instant pack film (Polaroid Co., Japan, 667, ISO: 3000/36°, resolution 11–14 line pairs/mm) was used as a recording medium [22].

2 Results

2.1 Laser-generated cavitation bubbles near gelatin surface

Figure 2a,b shows the behavior of laser-induced cavitation bubbles at different distances from a gelatin surface. The

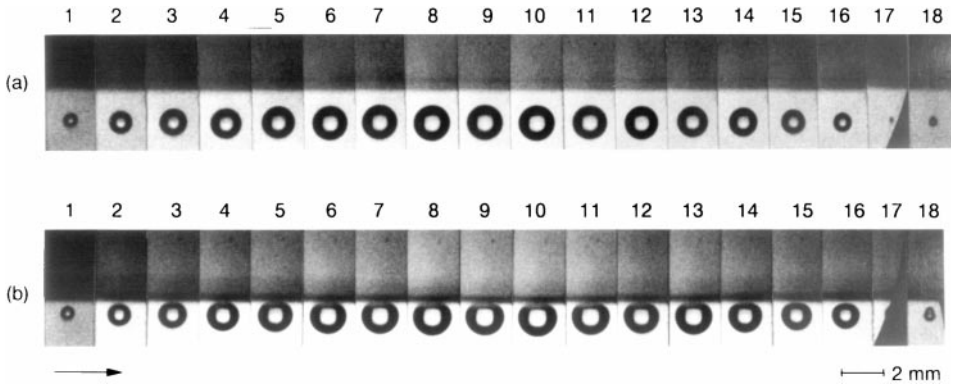

Fig. 2a,b. Collapse of a cavitation bubble near a gelatin surface. Interframe time 10 μs. Exposure time 2 μs. The direction of the laser beam was from below. **a** $R_{max} = 0.88$ mm, $L = 1.41$ mm, $L/R_{max} = 1.60$, $\tau = 169$ μs, $b_{R_{min}}/L = 1.09$, $c = 30\%$. **b** $R_{max} = 0.89$ mm, $L = 0.54$ mm, $L/R_{max} = 0.61$, $\tau = 182$ μs, $b_{R_{min}}/L = 1.27$, $c = 30\%$

weight of gelatin, c, was 30%. The interframe time was 10 μs, and the exposure time for each frame was 2 μs. Laser beams were focused into water from below. When a laser beam was focused into water, optical breakdown was induced, leading to plasma formation, shock wave emission, and cavitation bubble expansion. The cavitation bubble grew in a slightly elongated spherical shape perpendicular to the gelatin surface. The degree of a cavitation bubble deformation was small, compared with that of a cavitation bubble located at the same distance from a rigid surface [32]. The bubble continued to grow, reducing its internal pressure less than the equilibrium pressure which was determined by the non-condensable gas pressure, the vapor pressure, the surface tension of liquid, and the static pressure, and then finally reached its maximum volume in the ninth frame of Fig. 2a. The maximum bubble radius, R_{max}, was 0.88 mm. The relative distance defined as L/R_{max} was 1.60, where L was 1.41 mm from the gelatin surface. After that the bubble began to collapse, accelerated by the static pressure, reached its minimum size at the seventeenth frame of Fig. 2a. The bubble content of vapor and gas was strongly compressed, so that the bubble rebounded, resulting in a secondary shock wave emitting into the surrounding water. The period, τ, between the optical breakdown in water and the bubble rebound was measured to be 169 μs, which was determined by the interval between two pressure pulses generated at the optical breakdown and the bubble rebound. The bubble shape at the minimum volume was slightly elongated (see the seventeenth frame of Fig. 2a). The distance, $b_{R_{min}}$, between the center of the bubble with the minimum size and the gelatin surface was 1.53 mm. The relative migration distance from the surface, $b_{R_{min}}/L$, was 1.09, i.e. the bubble marginally migrated away from the gelatin surface. For Fig. 2b, $R_{max} = 0.89$ mm, $L = 0.54$ mm, $L/R_{max} = 0.61$, $\tau = 182$ μs, and $b_{R_{min}}/L = 1.27$. In this case, the bubble contacted the gelatin surface during the bubble expansion phase. The bubble grew in a slightly elongated shape, pressing the gelatin surface, and migrated away from the surface during the collapse phase. The migration from a surface is also observed for a free surface [15]. When a cavitation bubble collapses near a rigid of free surface, a liquid jet is formed within the bubble [3, 15, 16]. However, the liquid jet formation within a bubble near a gelatin surface was not clearly observed.

Figure 3 shows an example of bubble migration significantly away from the gelatin surface, where $R_{max} = 0.66$ mm, $L/R_{max} = 0.23$, $c = 20\%$, $b_{R_{min}}/L = 3.1$. The bubble grew in an oblate shape, strongly pressing the gelatin surface during the expansion phase, and then collapsed in a bell-shape. After the bubble rebounded, the bubble migrated away from the surface in an elongated slender shape. The gelatin surface was lifted with the sink flow induced by the collapsing bubble as seen in the thirteenth frame of Fig. 3. That is, the gelatin surface deformed obediently due to the pressure gradient that was generated by the source and sink flows from the bubble motion. The similar bubble behavior was observed near a rubber membrane, which was one of elastic boundaries [14, 22, 27, 28]. In the fourteenth frame, the bubble was split into two bubbles, that is, the phenomenon called "pinch-off" was observed [22].

Figure 4 indicates characteristic cavitation bubble migration from the gelatin surface for a different relative distance of L/R_{max}. The migration of a cavitation bubble from a free surface [15] was also shown in the same figure. The solid line was obtained by an image theory with point sinks and sources [33]. For a free surface, the degree of bubble migration increased with decreasing L/R_{max}. The bubbles near a gelatin surface showed a similar migratory character. The migration became significant as L/R_{max} was less than one, and then the bubble received a repulsive force from the gelatin surface. The response at a free surface is governed by inertial forces, whereas, near a gelatin surface elastic, restoring forces also contribute to the bubble dynamics.

Figure 5 shows that the period, τ^*, of the motion of a cavitation bubble near a gelatin surface for a different relative distance of L/R_{max}, where τ^* was a normalized time which was obtained by twice the Rayleigh's collapse time, $2T_c$, [34]

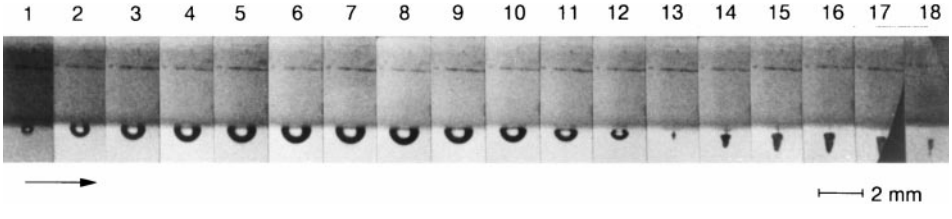

Fig. 3. Significant example of cavitation bubble migration away from the gelatin surface. Interframe time 10 μs. Exposure time 2 μs. The direction of the laser beam was from below. $R_{max} = 0.66$ mm, $L = 0.15$ mm, $L/R_{max} = 0.23$, $\tau = 124$ μs, $b_{R_{min}}/L = 3.1$, $c = 20\%$

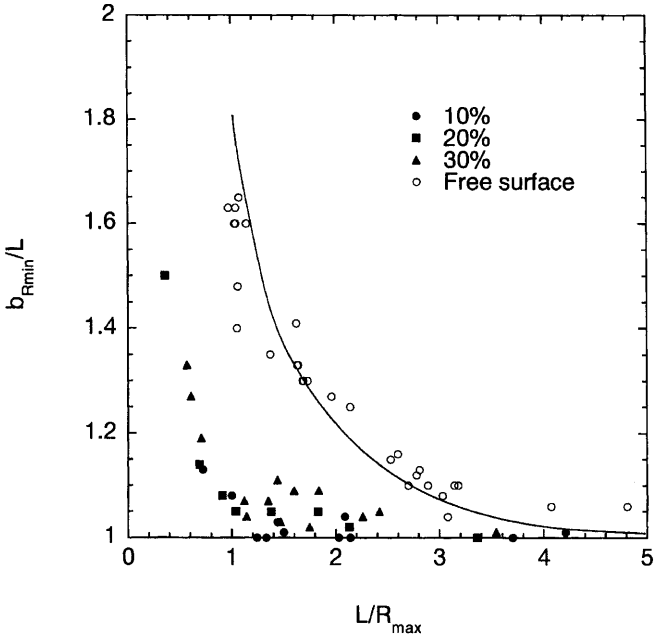

Fig. 4. Characteristic cavitation bubble migration, $b_{R\min}/L$, from the gelatin surface for a different relative distance of $L/R_{\max}$. ●: $c = 10\%$, ■: $c = 20\%$, ▲: $c = 30\%$, ○: free surface. The *solid line* was obtained by an image theory [15]

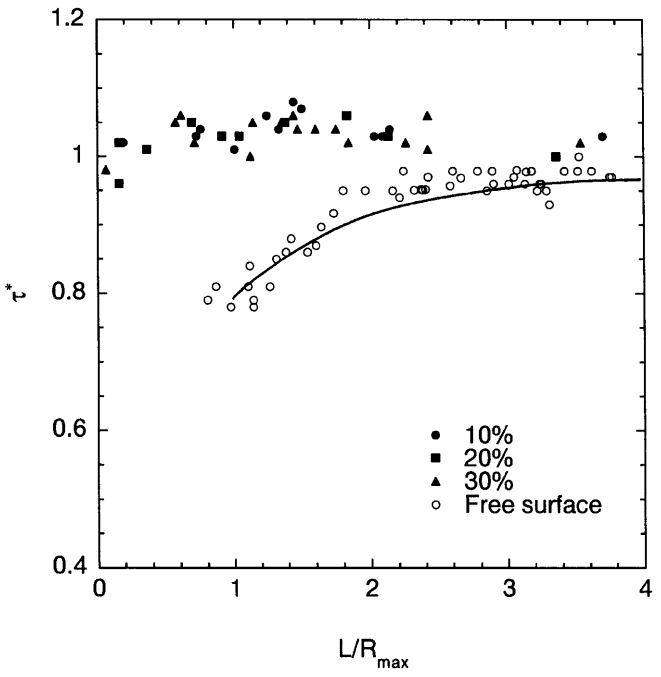

Fig. 5. Period of the motion, τ^*, of a cavitation bubble near a gelatin surface for a different relative distance of $L/R_{\max}$, which was normalized by the period of bubble in infinite volume. ●: $c = 10\%$, ■: $c = 20\%$, ▲: $c = 30\%$, ○: free surface. The *solid line* was obtained by an image theory [15]

given as

$$T_{\mathrm{c}} = 0.915 R_{\max} \sqrt{\frac{\rho_0}{P_0 - P_v}} \,. \tag{4}$$

The period of a cavitation bubble near a free surface [15] is indicated in the same figure. The period of a cavitation bubble near a free surface was shorter than that in the infinite volume of water, decreasing with decreasing the relative distance from the surface. The rate of period decrease was 20% at $L/R_{\max} = 1$. While the period of a cavitation bubble near a gelatin surface was slightly prolonged than that of twice the Rayleigh's collapse time for a wide range of $L/R_{\max}$. For $L/R_{\max} \approx 0$, the sink flow at the end of the cavitation bubble collapse raises the gelatin surface, resulting in a tensile force between the bubble and the surface. This tensile force and the source flow resulted from the bubble rebound related to the decrease in the bubble collapse time.

2.2 Interaction of bubbles attached to gelatin surfaces with shock waves

Figure 6a,b shows the collapse of air bubbles attached to gelatin surfaces with shock waves. The direction of the laser-induced shock wave propagation was vertically upward on the central axis of the bubble. The period of motion of the laser-induced cavitation was larger than that of the collapse time of the attached bubble with the laser-induced shock wave. Thus, the effect of the laser-induced cavitation bubble on the characteristics of the attached bubble was ignored. We confirmed that the shock wave impact produced no appreciable damage pit on the gelatin in the absence of a bubble. In Fig. 6,

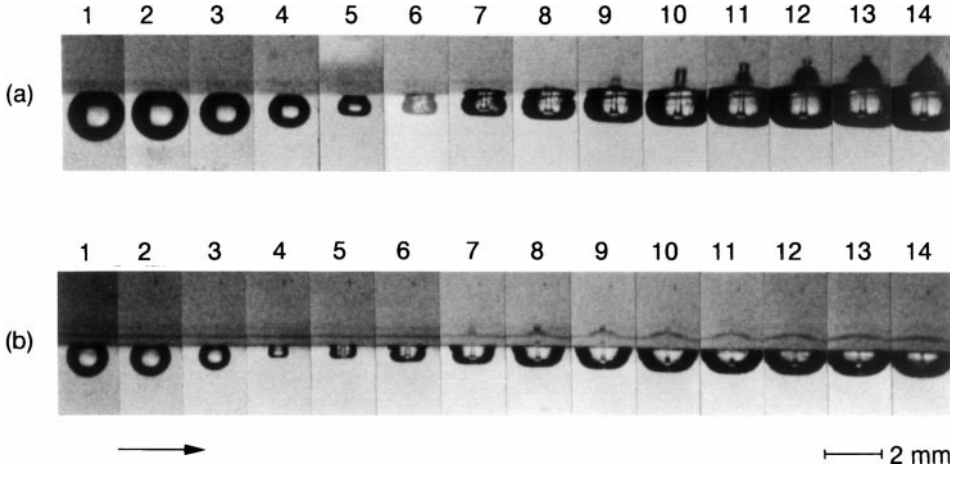

Fig. 6a,b. Collapse of an air bubble attached to a gelatin surface with a shock wave. Interframe time 10 μs. Exposure time 2 μs. The direction of the shock wave was from below. **a** $c = 10\%$, $R_{\mathrm{e}} = 1.05$ mm, $P_{\mathrm{s}} = 4.0$ MPa, $E_{\mathrm{c}} = 8.1$ mJ, $R_{\max} = 3.93$ mm, $L/R_{\max} = 1.91$. **b** $c = 30\%$, $R_{\mathrm{e}} = 0.76$ mm, $P_{\mathrm{s}} = 3.8$ MPa, $E_{\mathrm{c}} = 6.5$ mJ, $R_{\max} = 3.68$ mm, $L/R_{\max} = 2.04$

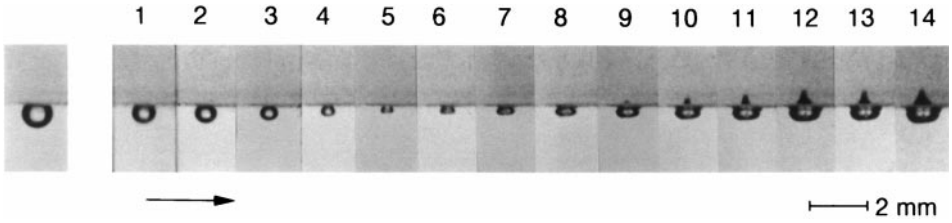

Fig. 7. Process of the liquid jet formation after shock wave interaction. Interframe time 2 μs. Exposure time is 0.4 μs. $c = 20\%$, $R_e = 0.56$ mm, $P_s = 4.2$ MPa, $E_c = 9.7$ mJ, $R_{max} = 4.17$ mm, $L/R_{max} = 1.80$

the initial bubble radii, R_e, were 1.05 mm and 0.76 mm, with overpressures of 4.0 MPa and 3.8 MPa, respectively. The particle velocity, u_p, behind the shock front for each case was calculated at 2.4 m s^{-1} and 2.5 m s^{-1}, respectively using the one-dimensional momentum equations [35]. Mach number was 1.003, where the sound velocity of water at 291 K was 1477 m s^{-1}. The speed of the shock wave was very close to the acoustic limit.

When the shock wave reached the bubble interface as a free surface, the free surface boundary condition required that the stress returned to zero, because of large impedance mismatch. A rarefaction wave was reflected back into the water, releasing the pressure and accelerating the bubble in the direction of the shock wave. The transmitted shock wave in the bubble was very small due to the impedance mismatch between the air and water. The bubble was transformed from a spherical to a flattened shape (see fifth frame of Fig. 6a), subsequently a liquid jet was formed within the bubble. The initial velocity of the bubble deformation, immediately after the shock wave impacted on the bubble surface, was calculated at twice the particle velocity ($= 2u_p$) behind the shock front since the changes in density in water were supposed to be infinitesimal. On the symmetric axis, the bubble surface deformed remarkably, developing to form the liquid jet whose velocity increased, especially during the late stage of the bubble collapse due to the convergence of water toward the bubble, because the rarefaction wave caused the pressure gradient [8, 36]. The jet penetrated through the downstream bubble wall, and finally impacted on the gelatin surface (see the sixth frame of Fig. 6a and the fifth frame of Fig. 6b). The configuration of the jet was nearly conical with a slightly rounded nose. The radius of the liquid jet was about one tenth of the radius of the initial bubble radius [3]. The jet continued to penetrate into the gelatin, reaching a constant penetration depth. The damage pit due to the liquid jet penetration was observed on the gelatin surface. It has been reported that the damage radius on the gelatin surface increased with increasing radius of the attached initial bubble [8]. Tomita and Shima [3] have shown that there is an "optimum bubble size" which yields a maximum jet velocity induced by the interaction of a shock wave with a gas bubble.

Figure 7 shows the process of the liquid jet formation after shock wave interaction. The interframe time was 2 μs, and the exposure time for each frame was 0.4 μs. The bubble reached the minimum volume at the fifth frame of Fig. 7. The initial bubble radius, R_e, was 0.56 mm, with an overpressure of 4.2 MPa. We could not conclude whether the liquid jet penetrated through the downstream bubble wall before or after the bubble reached its minimum volume.

Figure 8a–c shows the collapse of a bubble near gelatin surfaces having different weights; $c = 10\%$–30%. The pressure values and the bubble radii for each case were almost the same values; $P_s = 3.4$–3.5 MPa and $R_e = 0.66$–0.69 mm. The degree of the penetration depth and the degree of the

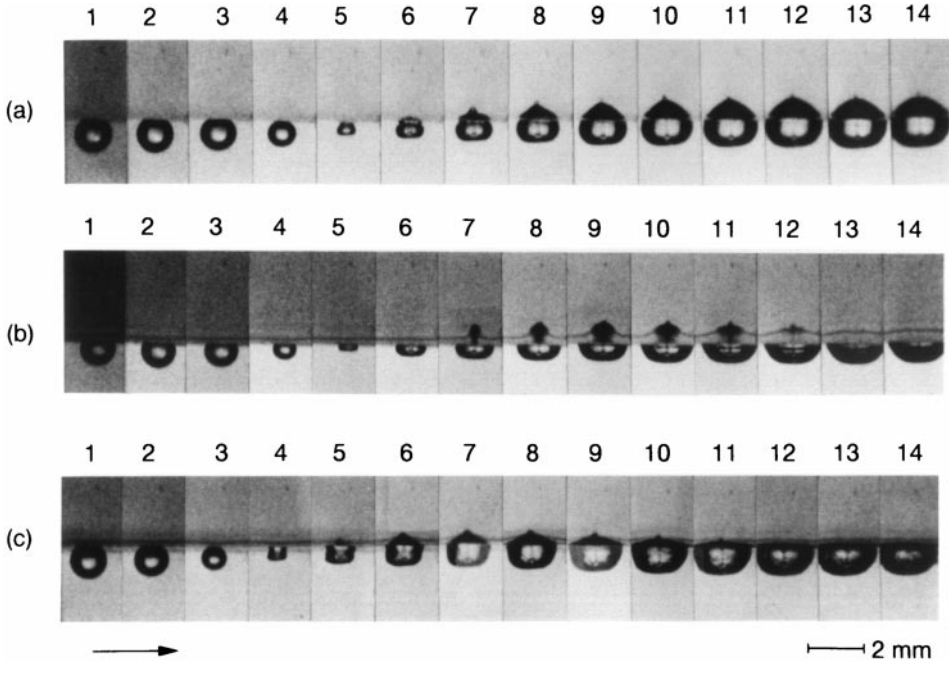

Fig. 8a–c. Collapse of an air bubble attached to a gelatin surface with different weights of gelatin. Interframe time 10 μs. Exposure time 2 μs. **a** $c = 10\%$, $R_e = 0.69$ mm, $P_s = 3.4$ MPa, $E_c = 4.5$ mJ, $R_{max} = 3.21$ mm, $L/R_{max} = 2.34$. **b** $c = 20\%$, $R_e = 0.66$ mm, $P_s = 3.5$ MPa, $E_c = 4.9$ mJ, $R_{max} = 3.34$ mm, $L/R_{max} = 2.25$. **c** $c = 30\%$, $R_e = 0.69$ mm, $P_s = 3.5$ MPa, $E_c = 4.9$ mJ, $R_{max} = 3.34$ mm, $L/R_{max} = 2.25$

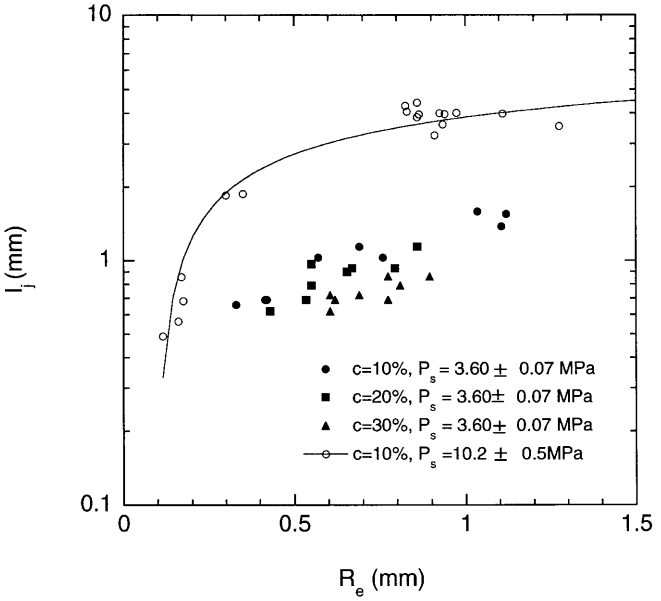

Fig. 9. Relation between the penetration depth of the liquid jet, l_j, and the bubble radius, R_e. $R_e = 0.33$–1.12 mm. $P_s = 3.60 \pm 0.07$ MPa, $E_c = 5.5 \pm 0.1$ mJ, $R_{max} = 3.47 \pm 0.03$ mm, $L/R_{max} = 2.16$. ●: $c = 10\%$, ■: $c = 20\%$, ▲: $c = 30\%$. ○: P_s is 10.2 ± 0.5 MPa. The *curves* were obtained by logarithmic approximation (ESWL experiment) [8]

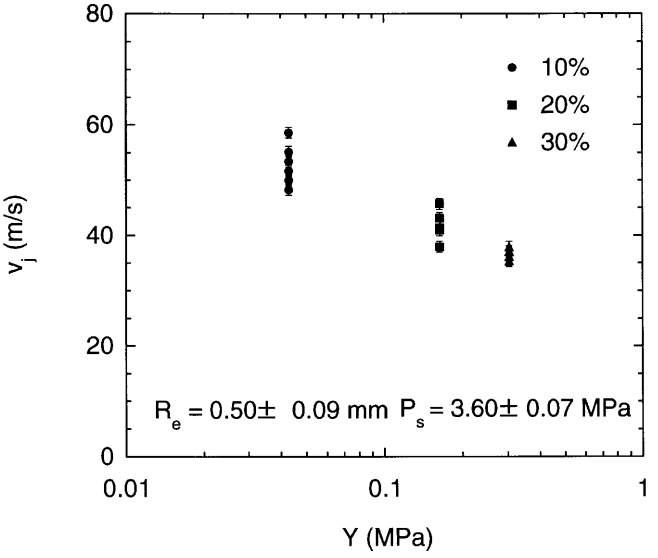

Fig. 10. Liquid jet velocity, V_j, penetrating into the gelatin for different Young's modulus, Y, of the gelatin. ●: $c = 10\%$, ■: $c = 20\%$, ▲: $c = 30\%$. $R_e = 0.50 \pm 0.09$ mm, $P_s = 3.60 \pm 0.07$ MPa, $E_c = 5.5 \pm 0.1$ mJ, $R_{max} = 3.47 \pm 0.03$ mm, $L/R_{max} = 2.16$

subsequent deformation of the gelatin surfaces due to the bubble expansion decreased with the increasing weight of gelatin.

Figure 9 shows the relation between the penetration depth of the liquid jet, l_j, and the initial bubble radius, R_e for different weights of gelatin; $R_e = 0.33$–1.12 mm; $c = 10\%$ (●), $c = 20\%$ (■), $c = 30\%$ (▲). The overpressures, P_s, of the shock waves were kept at 3.6 ± 0.07 MPa. The results obtained by Kodama and Takayama [8] using $P_s = 10.2 \pm 0.5$ MPa (ESWL experiment) and 10% weight of gelatin are also indicated in Fig. 9. For $P_s = 3.6 \pm 0.07$ MPa, the penetration depth increased with increasing the initial bubble radius. The degree of the penetration became larger for a lower weight of gelatin. In the case of $P_s = 10.2 \pm 0.5$ MPa, the penetration depth increased rapidly with increasing the initial bubble radius, approaching a constant value. The ratio of the overpressures for the two cases was about 2.8. It appears that the penetration depth is no longer independent of the overpressures of shock waves when it reaches its maximum value because the bubble has a finite volume. When the size of the bubble is extremely small, the liquid jet does not become a dominant factor for causing damage. It is noted that the initial condition of the collapsing bubble is affected by the difference between the profile of the laser-induced shock wave and that of ESWL.

Figure 10 shows that the liquid jet velocity penetrating through the gelatin for different weights of gelatin. The overpressure was 3.6 ± 0.07 MPa, and the calculated induced particle speed after the shock front was $2.2\ \mathrm{m\,s^{-1}}$. The axis of abscissas indicates the Young's modulus of the gelatin employed. The velocity was the mean value measured by dividing the penetration depth of the liquid jet into the gelatin from the initial penetration by 10 μs. Data was obtained from the pictures taken by 500 000 frames $\mathrm{s^{-1}}$ (Fig. 7). The jet velocity decreased with increasing the weight of gelatin, varying from $60\ \mathrm{m\,s^{-1}}$ to $35\ \mathrm{m\,s^{-1}}$. The decrease in the velocity corresponded to the increase in the fracture stress of the gelatin. The initial velocity of the bubble deformation with the impact of a shock wave was calculated at twice the particle velocity ($= 4.4\ \mathrm{m\,s^{-1}}$). Thus, the convergence effect due to the bubble collapse increases the liquid jet speed by a factor of $8.0 - 13.6$.

The counterjet is a jet flow in the opposite direction to the main jet [37]. Figure 11 shows a typical example of the counterjet formation. The bubble interacting with the shock wave expanded after the rebound, while the liquid jet penetrating into the gelatin returned back to the upper stream. It seems that the penetrating liquid jet is expelled by the gelatin. The prolonged counterjet, as shown in Fig. 11, was observed only for the weight of gelatin of 30%. And the counterjet was not observed to be less than the overpressure of 2.8 MPa. It is said that the counterjet formation is related to shock wave pressure, bubble size, and dynamic properties of the boundaries.

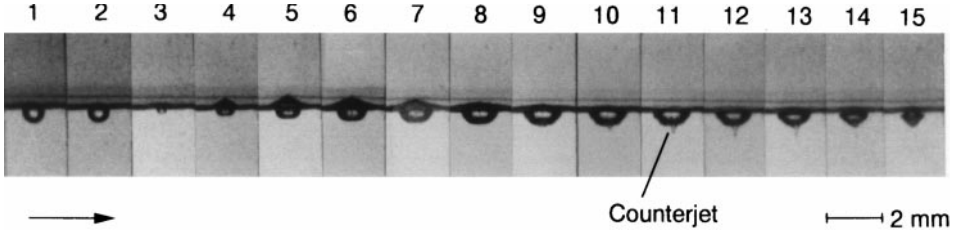

Fig. 11. Counter jet formation induced by the interaction of a shock wave. $c = 30\%$, $R_e = 0.40$ mm, $P_s = 2.8$ MPa, $E_c = 2.2$ mJ, $R_{max} = 2.60$ mm, $L/R_{max} = 2.88$

3 Discussion

3.1 Bubble migration

The normal force on and the normal velocity of the gelatin surface of marked particles were calculated throughout the bubble period using Rayleigh's analysis [34] and (1) and (2). Consider an initially plane surface $0.5R_{\max}$ away from the point of inception of the bubble, and assume the impulse pressure resulted from the bubble motion as a rectangle pulse. The total force $F(t)$ acting on the marked particles from the bubble side of the liquid was determined so that it was equal to the impulse during the period of bubble motion. The average normal displacement η' of the particles subtended by the circular area of the radius $R_{\max}$ were calculated using (1). These quantities for each gelatin concentration are shown as a function of time in Fig. 12 for the whole lifetime of a Rayleigh bubble. In the case of the gelatin surface of 10%, the displacement phase of the gelatin was similar to that of the infinite volume of the water, and the displacement at the end of the bubble period returned to the initial position $\eta' = 0$, i.e. the liquid particles near the gelatin surface behaved as if there were no surfaces near them, inducing no bubble migration. At the same time, the gelatin surface of 20% and 30% migrated to the point of the bubble inception, reducing the relative distance between the bubble and the surface. Thus, a decrease in the relative distance resulted in the flows towards to the bubble, leading to the bubble migration away from the surface.

The Kelvin impulse corresponds to the local momentum of the cavitation bubble and can therefore be used to determine aspects of the whole bubble motion. The Kelvin impulse obtains negative and positive limits for a rigid and a free surface, respectively [38]. When the Kelvin impulse obtains zero, the bubble motion and the subsequent surface displacement do not induce any forces over the bubble motion. This results in the state of neutral bubble collapse where no essential migration occurs, neither towards nor away from a surface [14]. At this condition the bubble at the end of the bubble collapse is a dumbbell shape, which is very similar to that of a bubble collapsing between two rigid surfaces [39].

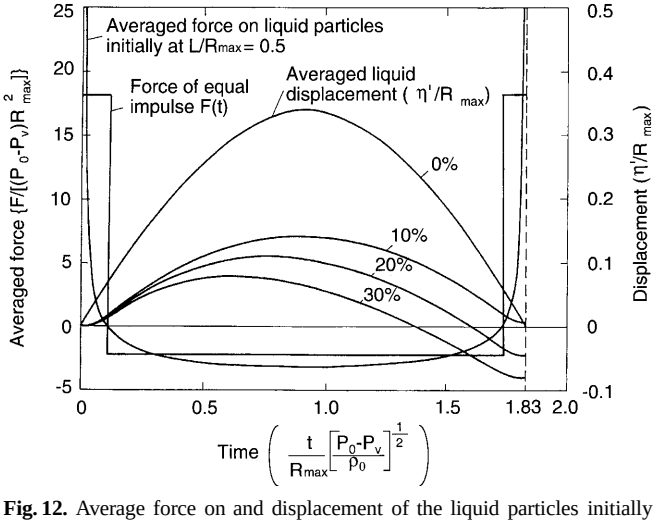

Fig. 12. Average force on and displacement of the liquid particles initially laying in a plane gelatin surface at a distance $L/R_{\max} = 0.5$ from a pulsating Rayleigh bubble

The bubbles near a gelatin surface with different concentration tend to stay at their generation points for almost the whole of their lifetime when $L/R_{\max} > 1$. Consequently, the subsequent gelatin surface displacement does not induce significant forces over the bubble, resulting in a zero Kelvin impulse, whereas, the bubble migration increases as $L/R_{\max}$ decreases less than one. The Kelvin impulse tends to obtain a higher positive value as $L/R_{\max}$ decreases. From the obtained results, it is assumed that in vivo cavitation bubbles tend to migrate away from the tissue surface due to the oscillatory bubble motion and the subsequent tissue displacement. Tissue will be displaced forcedly and subsequently damaged depending on the degree of the displacement and the displacement acceleration.

3.2 Period of bubble motion

The period of the motion of a bubble near a gelatin surface was slightly longer than that of a bubble in infinite of volume of water, except for $L/R_{\max} \approx 0$. The period of bubble motion near a rigid surface is symmetric with respect to that for a free surface around the axis of $\tau^* = 1$ by the image theory (see Fig. 5) [33]. The period for a rigid surface increases with decreasing the relative distance due to the water retardation near the surface. The gelatin surface restricts the inward water flow at the lower bubble wall. However, the degree of the restriction is quite small compared with a rigid surface, because of the deformation of the surface according to the bubble motion (see thirteenth frame of Fig. 3).

Figure 12 shows that the migration of bubbles from the surface increases with an increase in the weight of the gelatin. This suggests that the period of the bubble collapse decreases with the increase in the weight of the gelatin, because the bubble wall close to the gelatin surface is exposed to the increased stagnation pressure from the greater weight of the gelatin. In Fig. 5, the period of the bubble motion is shorter than twice the Rayleigh's collapse time near $L/R_{\max} \approx 0$.

3.3 Liquid jet formation

By increasing the stand-off distance from a rigid surface, the degree of the non-symmetric factor surrounding the bubble decreases, therefore the time of the jet formation approaches remove that of the bubble minimum volume. However, the time that the liquid jet penetrates through the downstream surface of the collapsing bubble is before the bubble rebound at $L/R_{\max} = 2$ from a solid surface [40]. The torus bubble that is penetrated by the liquid jet continues to collapse. When a liquid jet penetrates through the downstream bubble surface, the liquid jet interacts with the liquid particles converging on the bubble. The side of the liquid jet flows upstream, forming vortexes and pushing up the downstream bubble wall, that is, a "splash" is formed [22]. Blake et al. [41] numerically investigated the formation of the splash phenomena assuming the liquid was an incompressible flow. It was shown that the increase in vortex vectors and the decrease in the bubble volume were due to the splash. In a realistic flow field, when the liquid jet hits the downstream surface of the collapsing bubble, a shock wave is generated and the part of the kinetic energy

of the liquid jet is used for the shock wave emission [40]. Multi-effects such as liquid jet penetration, splash, and shock waves due to both the bubble rebound and the liquid jet impact, are associated with the bubble behavior at the end of the collapse.

In the present experiment, liquid jets are not clearly observed when cavitation bubbles collapsed at a distance of $L/R_{\max} = 0.61$–1.60 from a gelatin surface (see Fig. 2). At a distance of $L/R_{\max} = 0.23$, the bubble was split into two bubbles, that is, the "pinch-off" was observed (see Fig. 3). The formation of the splash phenomena was not clearly observed for a wide range of $L/R_{\max}$ from the gelatin surface having different weights. Each tissue has different dynamic properties. The tensile strength, for example, is 0.057 MPa for human's renalparenchyma, 0.52 MPa for human's stomach, 0.74–0.9 MPa for human's small intestine, 0.66–0.9 MPa for human's large intestine, 1.1–1.6 MPa for human's elastic aorta, 3.4 MPa for human cornea [29]. Systematic research on the liquid jet formation needs to be investigated further, based on the dynamic properties of elastic boundaries.

3.4 Shock waves

When a cavitation bubble is generated, a shock wave termed the primary shock wave is generated. Also, when a cavitation bubble rebounds, a secondary shock wave is produced. In some cases, the value of the secondary shock wave pressure is higher than that of the primary one [3]. For theoretical spherical acoustic propagation, the pressure front gradually steepens, but the wave attenuates approximately in proportional to r^{-1} through the liquid (r: radial distance from the center of the bubble) because energy dissipation and spreading of the pulse width are neglected [42–44]. In a realistic shock wave emission, the exponent of r is less than -1 in the range of a few hundred μm near the shock wave generation point [45–47].

It is assumed that the pressure value induced by the cavitation bubble near a gelatin surface at any $L/R_{\max}$ is close to that of a bubble in infinite volume of water, because the period of the bubble near the gelatin surface is slightly longer than that of a bubble in infinite volume of water. Tomita and Shima [48] have calculated the impulse pressure of a bubble in a viscous compressible liquid, and demonstrated that a bubble of 1 mm in radius can generate pressures up to thousands of MPa at the bubble surface, depending on the rate of non-condensable gas pressure and temperature. Tissues surrounding cavitation bubbles will be inevitably exposed to high impulsive pressures.

3.5 Liquid jet velocity with shock waves

The initial velocity of the bubble deformation with the impact of a shock wave was calculated at twice the particle velocity. In the present experiment, the calculated initial velocity of the bubble deformation was $4.4\,\mathrm{m\,s^{-1}}$ when the interaction of a bubble of 0.33–1.12 mm with an overpressure of 3.6 MPa was conducted. The measured liquid jet velocity at the gelatin surface varied from $35\,\mathrm{m\,s^{-1}}$ to $60\,\mathrm{m\,s^{-1}}$ (see Fig. 10). The convergence effect due to the bubble collapse increases the liquid jet speed by a factor of 8.0 to 13.6 (see Fig. 10). Philipp et al. [7] has reported that the jet velocity increased by a factor of 5 to 10 when bubbles of radii of 0.15 to 1.2 mm were interacted with electrohydraulic lithotripter-generated shock waves. The overpressure was 65 MPa and the width of the positive pulse was 800 ns. Kodama and Takayama [8] have shown that the liquid jet velocity increased by a factor of 12 when a bubble with a radius of 0.9 ± 0.3 mm was interacted with an explosive-generated shock wave. The overpressure was 10.2 ± 0.3 MPa and the width of the positive pulse was 666 ns. The explosives have been used as shock wave sources in ESWL [49]. The increase ratio in the present experiment using laser-induced shock waves agreed with the reported values in ESWL. In the near field of the laser breakdown, the remaining gas bubbles interact with the laser-induced shock wave and the subsequent expanding cavitation bubble. These events may show different characteristics of tissue damage mechanism from the present paper.

3.6 Liquid jet penetration

The interaction of shock waves with bubbles developed liquid jets directed to the gelatin surface. The liquid-jet-induced tissue damage during intracorporeal shock lithotripsy, ESWL, and intraocular photodisruption, may be resulted from the interaction of the remaining bubbles with intermittent shock waves. From Fig. 9, a bubble of 0.33–1.12 mm in initial radius produced about a 1-mm penetration depth by the interaction of an overpressure of 3.60 ± 0.07 MPa. The penetration velocity was varied from $35\,\mathrm{m\,s^{-1}}$ to $60\,\mathrm{m\,s^{-1}}$ (see Fig. 10). When the overpressures increased up to 10 MPa, the penetration depth of a few mm was obtained (see Fig. 9). Thus, a few mm penetration into tissue will occur as a result of the interaction of shock waves with bubbles. However, if the size of the bubble is extremely small, the liquid jet does not become a dominant factor for causing damage (see Fig. 9).

Liquid jets are high-speed material flows. When shock waves propagate into tissue, material flows are also induced behind the shock fronts. Now consider a plane shock wave moving with a constant velocity U_s into a tissue at rest pressure P_0 and density ρ_0. Conservation of momentum requires $P - P_0 = \rho_0 U_s u_p$, where P and u_p are the pressure, and material velocity of the tissue trailing the shock wave. When shock waves of 6–25 MPa with a pulse duration of about 500 ns propagate into rats' livers, cell elongation and split in the direction of the shock wave have been observed histologically [50]. Using the above equation, the induced material velocity behind the shock front is calculated at 3.9–$16.5\,\mathrm{m\,s^{-1}}$, where $P_0 = 101.3\,\mathrm{kPa}$, $\rho_0 = 993\,\mathrm{kg\,m^{-3}}$ (density of water at 310 K), $U_s = 1524\,\mathrm{m\,s^{-1}}$ (the sound velocity of water at 310 K). In this experiment, the jet velocity of 35–$60\,\mathrm{m\,s^{-1}}$ was obtained. If liquid jets of 35–$60\,\mathrm{m\,s^{-1}}$ with a certain duration time penetrate into tissue, the similar cell elongation and split phenomena will be observed. Kodama and Takayama [8] have shown that when a liquid jet of the order of $100\,\mathrm{m\,s^{-1}}$ penetrates into rats' livers, the elongation and split of nuclei in the liver parenchymal cells are generated due to the shear force in the direction of the liquid jet, since tissue is inhomogeneous and cells have complete organelles with different densities.

3.7 Liquid jet impact

The water hammer pressure, P_w, is given for liquid–solid impact as

$$P_w = V_j \rho_1 C_1 \rho_2 C_2 / (\rho_1 C_1 + \rho_2 C_2) \,, \tag{5}$$

where V_j is the liquid impact velocity and ρ_1, ρ_2, C_1, and C_2 are densities and shock wave velocities in the liquid and solid, respectively [51]. The compliance and the non-dimensional compliance are given by $Z = 1/\rho_2 C_2$ and $Z^* = Z\rho_1 C_1$, respectively. The impact pressure is rewritten as:

$$P_w = V_j \rho_1 C_1 / (Z^* + 1) \,. \tag{6}$$

The duration of this high pressure, τ_j, is given by

$$\tau_j = r_j / C_1 \,, \tag{7}$$

where r_j is the jet tip radius. Now, we assumed that the jet velocity at the moment when the liquid jet impacted at the gelatin surface was independent of the weight of the gelatin, and the jet velocity was $60\,\mathrm{m\,s^{-1}}$ (see Fig. 10). Also we assumed that the bubble radius was 0.5 mm, and the radius of the liquid jet was one tenth of the initial bubble radius, the calculated water hammer pressure was 46 MPa for 10%, 49 MPa for 20%, and 51 MPa for 30%. Each impact duration was calculated at 34 ns, where the density of water was $997.99\,\mathrm{kg\,m^{-3}}$ and the sound velocity was $1485.9\,\mathrm{m\,s^{-1}}$. With increasing acoustic impedance of the gelatin, the liquid jet impact increased; decrease in compliance of the targeted material increased the impact pressure of the liquid jet. When $Z^* \to 0$, then $P_w \to V_j \rho_1 C_1$, while the liquid jet can not penetrate into the surface with a certain compliance, and starts to flow along the surface in the radial direction. The jet impact increases to a value of $\approx 3 V_j \rho_1 C_1$ [52, 53] and the radial flow results in a different damage mechanism on the surface [3, 32]. The jet flows along the surface have been observed near stone models of renal and ureteral calculi [54], and they have also been pointed out near bovine cornea specimens by Vogel et al. [4] who demonstrated tissue damage due to the radial jet flow.

4 Conclusions

In this paper we have considered the growth and collapse of a cavitation bubble near a gelatin surface and the interaction of an air bubble attached to a gelatin surface with a shock wave to examine the behavior of in vivo cavitation bubbles and the subsequent tissue damage mechanism. The cavitation bubbles near the gelatin surface tended to migrate from the gelatin surface, and they were inclined not to produce liquid jets. Their lifetimes were prolonged to longer than that of twice the Rayleigh's collapse time for a wide range of relative distance, L/R_{max}, excepting for very small L/R_{max}. The interaction of an air bubble with a shock wave resulted in liquid jet directed to the gelatin surface, with tens of $\mathrm{m\,s^{-1}}$ at the gelatin surface. The impact pressure of tens of MPa at the gelatin surface was obtained, and the penetration depth of a few mm was achieved. The liquid jet had the potential to damage the gelatin surface.

The mechanisms of cavitation-bubble-induced tissue damage were closely related to the oscillatory bubble motion, the subsequent tissue displacement, and the liquid jet impact generated by the interaction of remaining cavitation bubbles with the intermittent shock waves. The mechanical damage process depended on the mechanical tissue properties.

Acknowledgements. The authors would like to acknowledge the advice of Professor Emeritus A. Shima of Tohoku University. We are grateful to Dr. A.G. Doukas and Dr. N.S. Nishioka of Wellman Laboratories of Photomedicine, Massachusetts General Hospital, Harvard Medical School who reviewed a rough draft of this article and provided many helpful suggestions.

References

1. A. Vogel, W. Hentschel, J. Holzfuss, W. Lauterborn: Ophthalmol. **93**, 1259 (1986)
2. A. Shima, K. Takayama, Y. Tomita, N. Miura: Acustica **48**, 293 (1981)
3. Y. Tomita, A. Shima: J. Fluid Mech. **169**, 535 (1986)
4. A. Vogel, P. Schweiger, A. Frieser, M.N. Asiyo, R. Birngruber: IEEE J. Quantum Electron. **QE-26**, 2240 (1990)
5. A.J. Coleman, J.E. Saunders: Ultrasonics **31**, 75 (1993)
6. M. Delius: Shock Waves **4**, 55 (1994)
7. A. Philipp, M. Delius, C. Scheffczyk, A. Vogel, W. Lauterborn: J. Acoust. Soc. Am. **93**, 2496 (1993)
8. T. Kodama, K. Takayama: Ultrasound Med. Biol. **24**, 723 (1998), Ultrasound Med. Biol. **24**, 1227 (1998)
9. P. Teng, N.S. Nishioka, W.A. Farinelli, R.R. Anderson, T.F. Deutsch: Lasers Surg. Med. **7**, 394 (1987)
10. H.J.C.M. Sterenborg, Th.M. de Reijke, J. Wiersma, R.C. Erckens, F.H.M. Jogsma: Urol. Res. **19**, 381 (1991)
11. A.J. Coleman, T. Kodama, M.J. Choi, T. Adams, J.E. Saunders: Ultrasound Med. Biol. **21**, 405 (1995)
12. R.K. Zeman, W.J. Davros, J.A. Goldberg, B.S. Garra, W.S. Hayes, E.L. Cattau, S.C. Horii, C.J. Cooper, P.M. Silverman: Radiology **177**, 163 (1990)
13. J.R. Blake, D.C. Gibson: J. Fluid Mech. **111**, 123 (1981)
14. A. Shima, Y. Tomita, D.C. Gibson, J.R. Blake: J. Fluid Mech. **203**, 199 (1989)
15. T. Kodama, Y. Tomita, A. Shima, R. Iwata: ASME FED-Vol. **116**, 27 (1991)
16. J.R. Blake, B.B. Taib, G. Doherty: J. Fluid Mech. **170**, 479 (1986)
17. Y. Tomita, A. Shima, T. Ohno: J. Appl. Phys. **56**, 125 (1984)
18. J.P. Dear, J.E. Field: J. Fluid Mech. **190**, 409 (1988)
19. T. Kodama, K. Takayama, N. Nagayasu: J. Appl. Phys. **80**, 5587 (1996)
20. T. Kodama, K. Takayama, H. Uenohara: Phys. Med. Biol. **42**, 2355 (1997)
21. Y. Tomita, T. Kodama, A. Shima: Appl. Phys. Lett. **59**, 274 (1991)
22. Y. Tomita, A. Shima: Acustica **71**, 161 (1990)
23. T. Kodama, Y. Tomita, A. Shima: Tran. Jpn. Soc. Mech. Eng. B **59**, 1431 (1993) (in Japanese)
24. S.A. Goss, R.L. Johnston, F. Dunn: J. Acoust. Soc. Am. **64**, 423 (1978)
25. W.J. Davros, B.S. Garra, R.K. Zeman: Radiology **178**, 397 (1991)
26. L. Kinsler, A.R. Frey, A.B. Coppens, J.V. Sanders: *Fundamentals of Acoustics*, 3rd edn. (Wiley, New York, Chichester, Brisbane, Toronto, Singapore 1982)
27. D.C. Gibson, J.R. Blake: Appl. Sci. Res. **38**, 215 (1982)
28. T. Kodama: Ph.D. Thesis, Tohoku University 1992 (in Japanese)
29. *Handbook of Bio-Medical Engineering* (Corona, Tokyo 1978) (in Japanese)
30. Y.C. Fung: *Biomechanics: Mechanical Properties of Living Tissues*, 2nd edn. (Springer, Berlin, Heidelberg 1993)
31. M.T. Carnell, P.T. Fiadeiro, D.C. Emmony: J. Acoust. Soc. Am. **97**, 677 (1995)
32. A. Philipp, W. Lauterborn: J. Fluid Mech. **361**, 75 (1998)
33. R.H. Cole: *Underwater Explosion* (Princeton University Press, Princeton 1948)
34. Lord Rayleigh: Philos. Mag. **34**, 94 (1917)
35. W.F. Ballhaus Jr., M. Holt: Phys. Fluid. **17**, 1068 (1974)
36. Z. Ding, S.M. Gracewski: J. Fluid Mech. **309**, 183 (1996)
37. A. Vogel, W. Lauterborn, R. Timm: J. Fluid Mech. **206**, 299 (1989)

38. J.R. Blake, P. Cerone: J. Austral. Math. Soc. **23**, 383 (1982)
39. A. Shima, Y. Sato: J. Appl. Math. Phys. (ZAMP) **31**, 691 (1980)
40. C.D. Ohl, A. Philipp, W. Lauterborn: Ann. Phys. **4**, 26 (1995)
41. J.R. Blake, Y. Tomita, R.P. Tong: Appl. Sci. Res. **58**, 77 (1998)
42. R. Hickling, M.S. Plesset: Phys. Fluids **7**, 7 (1964)
43. Y. Tomita, A. Shima: Bull. Jpn. Soc. Mech. Eng. **20**, 1453 (1977)
44. S. Fujikawa, T. Akamatsu: J. Fluid Mech. **97**, 481 (1980)
45. A.G. Doukas, A.D. Zweig, J.K. Frisoli, R. Birngruber, T.F. Deutsch: Appl. Phys. B **53**, 237 (1991)
46. B. Zysset, J.G. Fujimoto, T.F. Deutsch: Appl. Phys. B **48**, 139 (1989)
47. A. Vogel, S. Busch, U. Parlitz: J. Acoust. Soc. Am. **100**, 148 (1996)
48. Y. Tomita, A. Shima: ZAMM **59**, 297 (1979)
49. M. Kuwahara: Jpn. J. Endourol. ESWL **6**, 5 (1993)
50. T. Kodama, H. Uenohara, K. Takayama: Ultrasound Med. Biol. **24**, 1459 (1998)
51. F.J. Heymann: Trans ASME D, J. Basic Eng. **90**, 400 (1968)
52. F.J. Heymann: J. Appl. Phys. **40**, 5113 (1969)
53. M.B. Lesser, J.E. Field: Ann. Rev. Fluid Mech. **15**, 97 (1983)
54. P. Zhong, H.L. Tong, F.H. Cocks, G.M. Preminger: J. Endourol **11**, 55 (1997)